Research Article | Vol. 24, No. 14 / 11 July 2016 / OPTICS EXPRESS 15261

Optics EXPRESS

Saturable absorption of femtosecond optical pulses in multilayer turbostratic graphene

FANQI MENG,[1,*] MARK D. THOMSON,[1] FEDERICA BIANCO,[2] ANTONIO ROSSI,[3] DOMENICA CONVERTINO,[3] ALESSANDRO TREDICUCCI,[4] CAMILLA COLETTI,[3] AND HARTMUT G. ROSKOS[1]

[1]*Physikalisches Institut, J. W. Goethe-Universität, Max-von-Laue-Straße 1, D-60438 Frankfurt am Main, Germany*
[2]*NEST, Istituto Nanoscienze–CNR and Scuola Normale Superiore, P.za S. Silvestro 12, 56127 Pisa, Italy*
[3]*Center for Nanotechnology Innovation @NEST, Istituto Italiano di Tecnologia, P.za S. Silvestro 12, 56127 Pisa, Italy*
[4]*NEST, Istituto Nanoscienze–CNR and Dipartimento di Fisica "E. Fermi," Università di Pisa, Largo Pontecorvo 3, 56127 Pisa, Italy*
[*]*f.meng@physik.uni-frankfurt.de*

Abstract: We investigate the nonlinear transmission of a ~280-layer turbostratic graphene sheet for near-infrared amplifier laser pulses (775 nm, Ti:sapphire laser) with a duration of 150-fs and 20-fs. Saturable absorption is observed in both cases, however it is not very strong, amounting to ~13% transmittance change for the 20-fs (150-fs) pulses at a peak intensity of 30 GW/cm^2 (4 GW/cm^2). The dependence on incident peak intensity is reproduced well using a theoretical model for the time-dependent saturable absorption, where the excited carriers vacate the photo-excited energy range within 3-5 fs, which we attribute to energy redistribution due to carrier-carrier scattering. This is also supported by spectrally resolved measurements for the 20-fs pulses, which show a marked dependence of the degree of saturation on the photon energy. A key result is that the shorter pulses do not yield a lower saturation fluence, due to the combined effects of the broader excitation bandwidth, and the rapid and broad energy redistribution. We also predict the potential performance of multilayer graphene samples for removing pedestal and pre-pulse structure from ultrafast high-energy pulses.

OCIS codes: (160.4236) Nanomaterials; (190.0190) Nonlinear optics; (190.4400) Nonlinear optics, materials.

References and links

1. S. Backus, C. G. Durfee, M. M. Murnane, and H. C. Kapteyn, "High power ultrafast lasers," Rev. Sci. Instrum. **69**(3), 1207–1223 (1998).
2. J. Bredenbeck, A. Ghosh, M. Smits, and M. Bonn, "Ultrafast two dimensional-infrared spectroscopy of a molecular monolayer," J. Am. Chem. Soc. **130**(7), 2152–2153 (2008).
3. H. G. Yan, D. H. Song, K. F. Mak, I. Chatzakis, J. Maultzsch, and T. F. Heinz, "Time-resolved Raman spectroscopy of optical phonons in graphite: phonon anharmonic coupling and anomalous stiffening," Phys. Rev. B **80**(12), 121403 (2009).
4. M. Nisoli, S. De Silvestri, O. Svelto, R. Szipocs, K. Ferencz, Ch. Spielmann, S. Sartania, and F. Krausz, "Multiphoton plasmon-resonance microscopy," Opt. Lett. **22**(8), 522–524 (1997).
5. G. Doumy, F. Quéré, O. Gobert, M. Perdrix, P. Martin, P. Audebert, J. C. Gauthier, J.-P. Geindre, and T. Wittmann, "Complete characterization of a plasma mirror for the production of high-contrast ultraintense laser pulses," Phys. Rev. E Stat. Nonlin. Soft Matter Phys. **69**(2), 026402 (2004).
6. A. Zhidkov, A. Sasaki, T. Utsumi, I. Fukumoto, T. Tajima, F. Saito, Y. Hironaka, K. G. Nakamura, K. Kondo, and M. Yoshida, "Prepulse effects on the interaction of intense femtosecond laser pulses with high-Z solids," Phys. Rev. E Stat. Phys. Plasmas Fluids Relat. Interdiscip. Topics 62(5 5 Pt B), 7232–7240 (2000).
7. F. Meng, M. D. Thomson, and H. G. Roskos, "Relativistic Doppler frequency upconversion of terahertz pulses reflecting from a photoinduced plasma front in silicon," Phys. Rev. B **90**(15), 155207 (2014).
8. K.-H. Hong, B. Hou, J. A. Nees, E. Power, and G. A. Mourou, "Generation and measurement of >10^8 intensity contrast ratio in a relativistic kHz chirped-pulse amplified laser," Appl. Phys. B **81**(4), 447–457 (2005).

#261437 http://dx.doi.org/10.1364/OE.24.015261
Journal © 2016 Received 21 Mar 2016; revised 4 May 2016; accepted 4 May 2016; published 27 Jun 2016

Optics EXPRESS

9. J. Itatani, J. Faure, M. Nantel, G. Mourou, and S. Watanabe, "Suppression of the amplified spontaneous emission in chirped-pulse-amplification lasers by clean high-energy seed-pulse injection," Opt. Commun. **148**(1–3), 70–74 (1998).
10. M. P. Kalashnikov, E. Risse, H. Schönnagel, and W. Sandner, "Double chirped-pulse-amplification laser: a way to clean pulses temporally," Opt. Lett. **30**(8), 923–925 (2005).
11. D. M. Gold, "Direct measurement of prepulse suppression by use of a plasma shutter," Opt. Lett. **19**(23), 2006–2008 (1994).
12. F. Zhang, S. Han, Y. Liu, Z. Wang, and X. Xu, "Dependence of the saturable absorption of graphene upon excitation photon energy," Appl. Phys. Lett. **106**(9), 091102 (2015).
13. Z. Zheng, C. Zhao, S. Lu, Y. Chen, Y. Li, H. Zhang, and S. Wen, "Microwave and optical saturable absorption in graphene," Opt. Express **20**(21), 23201–23214 (2012).
14. G. Xing, H. Guo, X. Zhang, T. C. Sum, and C. H. A. Huan, "The Physics of ultrafast saturable absorption in graphene," Opt. Express **18**(5), 4564–4573 (2010).
15. J. M. Dawlaty, S. Shivaraman, J. Strait, P. George, M. Chandrashekhar, F. Rana, M. G. Spencer, D. Veksler, and Y. Chen, "Measurement of the optical absorption spectra of epitaxial graphene from terahertz to visible," Appl. Phys. Lett. **93**(13), 131905 (2008).
16. M. Breusing, C. Ropers, and T. Elsaesser, "Ultrafast carrier dynamics in graphite," Phys. Rev. Lett. **102**(8), 086809 (2009).
17. Q. Bao, H. Zhang, Y. Wang, Z. Ni, Y. Yan, Z. X. Shen, K. P. Loh, and D. Y. Tang, "Atomic-layer graphene as a saturable absorber for ultrafast pulsed lasers," Adv. Funct. Mater. **19**(19), 3077–3083 (2009).
18. H. Yang, X. Feng, Q. Wang, H. Huang, W. Chen, A. T. S. Wee, and W. Ji, "Giant two-photon absorption in bilayer graphene," Nano Lett. **11**(7), 2622–2627 (2011).
19. W. D. Tan, C. Y. Su, R. J. Knize, G. Q. Xie, L. J. Li, and D. Y. Tang, "Mode locking of ceramic Nd:yttrium aluminum garnet with graphene as a saturable absorber," Appl. Phys. Lett. **96**(3), 031106 (2010).
20. Z. Sun, T. Hasan, F. Torrisi, D. Popa, G. Privitera, F. Wang, F. Bonaccorso, D. M. Basko, and A. C. Ferrari, "Graphene mode-locked ultrafast laser," ACS Nano **4**(2), 803–810 (2010).
21. C. C. Lee, J. M. Miller, and T. R. Schibli, "Doping-induced changes in the saturable absorption of monolayer graphene," Appl. Phys. B **108**(1), 129–135 (2012).
22. Q. Bao, H. Zhang, Z. Ni, Y. Wang, L. Polavarapu, Z. X. Shen, Q. Xu, D. Y. Tang, and K. P. Loh, "Monolayer graphene as a saturable absorber in a mode-locked laser," Nano Res. **4**(3), 297–307 (2011).
23. M. Amos, K. Fuse, and S. Yamashita, "Mechanical exfoliation of graphene for the passive mode-locking of fiber lasers," Appl. Phys. Lett. **99**(12), 121107 (2011).
24. C. L. Frewin, C. Coletti, C. Riedl, U. Starke, and S. E. Saddow, "A comprehensive study of hydrogen etching on the major SiC polytypes and crystal orientations," Mater. Sci. Forum **615–617**, 589–592 (2009).
25. F. Bianco, V. Miseikis, D. Convertino, J.-H. Xu, F. Castellano, H. E. Beere, D. A. Ritchie, M. S. Vitiello, A. Tredicucci, and C. Coletti, "THz saturable absorption in turbostratic multilayer graphene on silicon carbide," Opt. Express **23**(9), 11632–11640 (2015).
26. C. Faugeras, A. Nerrière, M. Potemski, A. Mahmood, E. Dujardin, C. Berger, and W. A. de Heer, "Few-layer graphene on SiC, pyrolitic graphite, and graphene: a Raman scattering study," Appl. Phys. Lett. **92**(1), 011914 (2008).
27. L. G. Cançado, A. Jorio, E. H. Ferreira, F. Stavale, C. A. Achete, R. B. Capaz, M. V. O. Moutinho, A. Lombardo, T. S. Kulmala, and A. C. Ferrari, "Quantifying defects in graphene via Raman spectroscopy at different excitation energies," Nano Lett. **11**(8), 3190–3196 (2011).
28. M. D. Thomson, V. Blank, and H. G. Roskos, "Terahertz white-light pulses from an air plasma photo-induced by incommensurate two-color optical fields," Opt. Express **18**(22), 23173–23182 (2010).
29. M. Currie, J. D. Caldwell, F. J. Bezares, J. Robinson, T. Anderson, H. Chun, and M. Tadjer, "Quantifying pulsed laser induced damage to graphene," Appl. Phys. Lett. **99**(21), 211909 (2011).
30. B. Semnani, A. H. Majedi, and S. Safavi-Naeini, "Nonlinear quantum optical properties of graphene," J. Opt. **18**(3), 035402 (2016).
31. R. R. Nair, P. Blake, A. N. Grigorenko, K. S. Novoselov, T. J. Booth, T. Stauber, N. M. R. Peres, and A. K. Geim, "Fine structure constant defines visual transparency of graphene," Science **320**(5881), 1308 (2008).
32. T. Kampfrath, L. Perfetti, F. Schapper, C. Frischkorn, and M. Wolf, "Strongly coupled optical phonons in the ultrafast dynamics of the electronic energy and current relaxation in graphite," Phys. Rev. Lett. **95**(18), 187403 (2005).
33. S. B. Lu, L. L. Miao, Z. N. Guo, X. Qi, C. J. Zhao, H. Zhang, S. C. Wen, D. Y. Tang, and D. Y. Fan, "Broadband nonlinear optical response in multi-layer black phosphorus: an emerging infrared and mid-infrared optical material," Opt. Express **23**(9), 11183–11194 (2015).
34. P. A. Obraztsov, M. G. Rybin, A. V. Tyurnina, S. V. Garnov, E. D. Obraztsova, A. N. Obraztsov, and Y. P. Svirko, "Broadband light-induced absorbance change in multilayer graphene," Nano Lett. **11**(4), 1540–1545 (2011).
35. D. Brida, A. Tomadin, C. Manzoni, Y. J. Kim, A. Lombardo, S. Milana, R. R. Nair, K. S. Novoselov, A. C. Ferrari, G. Cerullo, and M. Polini, "Ultrafast collinear scattering and carrier multiplication in graphene," Nat. Commun. **4**, 1987 (2013).

Optics EXPRESS

36. P. A. George, J. Strait, J. Dawlaty, S. Shivaraman, M. Chandrashekhar, F. Rana, and M. G. Spencer, "Ultrafast optical-pump terahertz-probe spectroscopy of the carrier relaxation and recombination dynamics in epitaxial graphene," Nano Lett. **8**(12), 4248–4251 (2008).
37. M. Breusing, S. Kuehn, T. Winzer, E. Malić, F. Milde, N. Severin, J. P. Rabe, C. Ropers, A. Knorr, and T. Elsaesser, "Ultrafast nonequilibrium carrier dynamics in a single graphene layer," Phys. Rev. B **83**(15), 153410 (2011).

1. Introduction

Continuous advances in amplifier-laser technology have given rise to commercialized, table-top, high-energy picosecond/femtosecond (ps/fs) lasers (with focal intensities approaching even PW/cm^2), which have been employed to explore high-energy light-matter interactions, such as higher-harmonic generation [1], molecular dynamics [2], as well as carrier dynamics in solid states materials [3]. By employing subsequent spectral broadening and recompression, one can obtain high-energy pulses in the sub-10-fs range [4]. However, it is well-known [5] that such amplifier laser pulses can suffer from the presence of a temporal pedestal about the main intensity peak as well as weaker pre-pulses from neighboring seed pulses leaking into the amplifier. This reduces the optical contrast of the pulses, which can have a deleterious effect on high-energy experiments due to the pre-excitation of the sample under study [6, 7]. As a representative example, in the relativistic Doppler experiments of Ref [7], any optical energy preceding the main pulse generates a weak pre-plasma, which partially absorbs the incoming probe pulse and greatly diminishes the Doppler frequency up-conversion efficiency. The temporal pedestal typically originates from the amplified spontaneous emission (ASE) that arises in the amplifier cavity. Also, pre-pulse/pedestal structure can be present on a fs/ps time scale about the main pulse due to residual spectral phase distortion of the ultra-short pulses. A number of different methods have been proposed to increase the optical contrast, e.g., using a semiconductor saturable absorber before the pulse amplification [8, 9], double chirped-pulse amplification [10], or external plasma shutters (plasma mirrors) [5, 11]. Monolayer and multilayer graphene saturable absorbers, as have been studied from the visible [12] to the microwave [13] spectral ranges, demonstrate a relatively low saturation intensity and high damage threshold, which could serve as an alternative for the cleaning of high-energy pulses after the laser cavity. However, the modulation depth of the transmittance has been limited because of the limited number of monolayers of the graphene samples which have been explored until now [12–23]. Thick turbostratic graphene is of interest to obtain a practically useful modulation depth.

In this contribution, we report about the investigation of the saturable absorption behavior of a multilayer turbostratic graphene specimen, determined to have ~280 graphene layers, by employing both 150-fs and 20-fs near-infrared pulses. Saturable absorption characteristics are observed in both cases and the experimental findings are well reproduced via a physical model which assumes that the charge carriers are brought out of the spectrally accessible range by carrier-carrier scattering processes occurring on a time scale of 2-4 fs. This assumption is supported by spectrally resolved measurements for the 20-fs pulses, which indicate a strong redistribution of the initially excited carriers during the pulse duration. The ultrafast relaxation explains why the shorter pulses do not yield a lower saturation fluence, despite the higher corresponding intensity. We also simulate the saturation and pulse shaping behavior of a 100-layer graphene stack for suppressing pre-energy/pedestals of high-energy pulses.

2. Graphene sample description

Multilayer turbostratic graphene was grown on semi-insulating, nominally on-axis 4H-SiC substrate purchased from Cree, Inc. Before growth, hydrogen etching was used to remove polishing scratches and to reveal atomic steps [24]. Growth was performed in a resistively heated cold-wall reactor (BM, Aixtron) similar to the procedure reported in Bianco et al. [25]. In this case, no carbon precursor was used, and growth was carried out via thermal

Optics EXPRESS

decomposition of SiC by heat treatment of the substrate in argon atmosphere (Ar flow set to 800 sccm and the pressure to 780 mbar) at a temperature of 1380°C for 8 minutes. The thickness and the quality of the sample were evaluated via micro-Raman spectroscopy, which was performed using a Renishaw InVia system equipped with a 532-nm green laser and a motorized stage for large-area mapping. Figure 1 depicts a Raman spectrum measured for the sample used in this study. The 2D peak is well-fitted with a single Lorentzian, thus confirming the decoupled nature of the individual graphene layers [26]. Furthermore, the low values of the intensity ratio I_D/I_G (i.e.,< 0.08) and the linewidth Γ_G (about 20 cm^{-1}) indicate that the sample is in the low-defect-density regime [27].

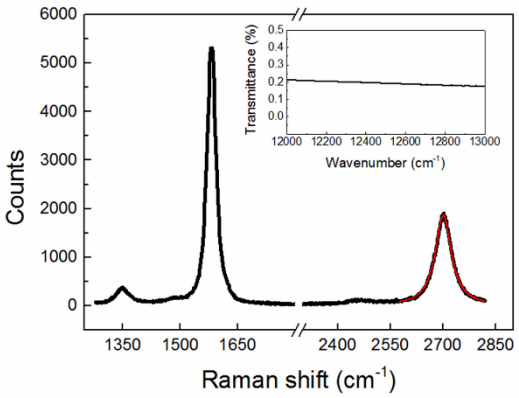

Fig. 1. Representative Raman spectrum of multilayer graphene on SiC measured at a wavelength of 532 nm. The red solid line is the single Lorentzian fit. The inset shows the transmittance spectrum of the graphene sheet measured by FTIR spectroscopy in the near-infrared.

3. Results and discussion

3.1. Saturable absorption vs. optical pulse duration

The absorption measurement setup is schematically shown in Fig. 2. Excitation by an unfocused beam was employed, as opposed to an open-aperture Z-scan technique [13]. In the latter case, the sample would be moved through the focus of the beam which was found to produce artifacts by contaminations, defects or microstructure inhomogeneities in the sample. By keeping the size and position of the illuminated spot on the sample unchanged, such structural features influence all measurements equally. The measurements were carried out with ultrashort near-infrared pulses with two different pulse durations. The 150-fs optical pulses were provided directly from the Ti:sapphire regenerative amplifier (Clark-MXR-CPA-2101, 775 nm, 1 kHz), which we refer to hereafter as the “CPA” pulses. Pulses with a ~20-fs duration were obtained by first spectrally broadening the CPA pulses in a hollow-core fiber (Femtolasers Kaleidoscope) in an argon-gas-filled chamber followed by re-compression via a sequence of negative-dispersion mirrors [28]; they are referred to hereafter as the “HCF” pulses. The optical pulse energy at the sample was varied with a half-wave plate followed by a thin-film polarizing beamsplitter. Behind this variable attenuator, a second beamsplitter was used to provide a reference beam for the graphene sample transmission. After the sample, both the reference and the sample beams were coupled either to two photodiodes (Thorlabs, DET 100A/M) or a fiber-coupled two-channel spectrometer (Ocean Optics S2000), before which additional neutral density filters could be inserted to ensure a linear detection response. The two photodiodes were calibrated with a power meter (Melles Griot 13PEM001) in order to provide pulse energy values. The beam diameter on the graphene was controlled through an iris, which determines the nominal beam diameter on the graphene sample to be 3 mm.

Optics EXPRESS

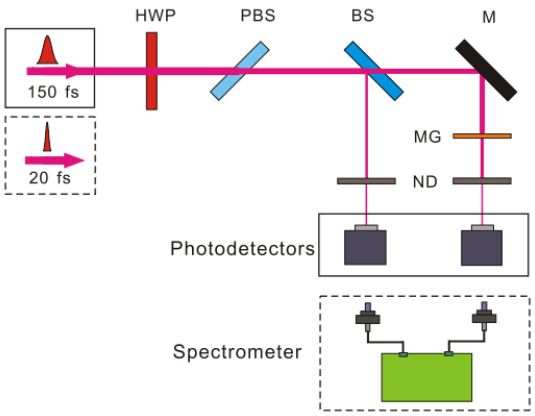

Fig. 2. Experimental setup for measuring the saturable absorption of graphene. HWP: half-wave plate, PBS: thin-film polarizing beamsplitter, BS: beamsplitter, M: mirror, MG: multilayer graphene, ND: neutral density filter.

The samples' transmittance, as measured by Fourier transform infrared (FTIR) spectroscopy from 783 nm to 833 nm and after correction for the substrate reflection is shown in the inset of Fig. 1. The spectral dependence is fairly flat as one would expect for graphene layers which do not interact (as demonstrated by Raman spectroscopy) and for the universal conductance of graphene. We now turn to the measurements with the ultrashort laser pulses. The transmittance of the graphene stack is presented as a function of peak intensity and fluence in Figs. 3(a) and 3(b), respectively. The reduced transmittance (T) plotted here is a direct measure of the absorbance (A = 1-T) of the graphene stack, as the reflectance of the air-graphene interface and the Fresnel reflections from the graphene-SiC and SiC-air interfaces have been eliminated from the raw transmittance data which vary across the sample from 0.06 to 0.09%. At low intensities, the mean value of the reduced transmittance is found to be ~0.15%, which indicates that there are about 280 graphene layers in the sample, assuming the universal absorption constant of 2.3% per layer and again assuming no significant coupling between the layers.

Considering the peak intensity (see Fig. 3(a)), the transmittance starts to show saturation at ~0.3 GW/cm^2 for CPA pulse excitation, while the saturation for the HCF pulse occurs at a factor ~10 higher (~3 GW/cm^2). The saturation intensity obtained for the CPA pulses is comparable with those of previous reports [14, 18] with similar photon energy and pump pulse duration, however, reports of the saturable absorption for shorter excitation pulses down to ~20 fs are absent in the literature.

For the highest intensities used here, the transmission enhancement is about 13% for both types of pulses. Note that we did not go to higher intensities here due to the onset of optical damage to the samples [29]. In order to address any possible substrate contribution to the observed saturation effect, we also measured the transmittance of a monolayer-graphene sample on a nominally equal SiC substrate. In this case, no saturable absorption was observable up to 100 GW/cm^2. For higher intensities, the transmission was actually observed to decrease, which can be explained by two-photon absorption (TPA) in the SiC substrate [14], which masks (and then dominates) the saturable absorption in the monolayer graphene. This TPA influence is not present in the multilayer graphene sample (Fig. 3) as the intensity reaching the substrate is limited by the absorption in the graphene. Interestingly, when the transmission is plotted vs. the pulse fluence (Fig. 3(b)), the data for both pulse durations nearly coincide. This result is not trivial, as the peak intensity of the HCF pulses is almost a factor 10 higher than that of the CPA pulses for the same fluence. One has to consider that the energy transmittance is an average over the duration of the pulse, involving the interplay of the temporal intensity profile and time-dependent carrier dynamics in the sample. As we will

Optics EXPRESS

find by the simulations to be addressed now, this independence of the saturation behavior from the pulse duration originates from extremely fast carrier relaxation occurring on time scales much shorter than 20 fs, the duration of the HCF pulses.

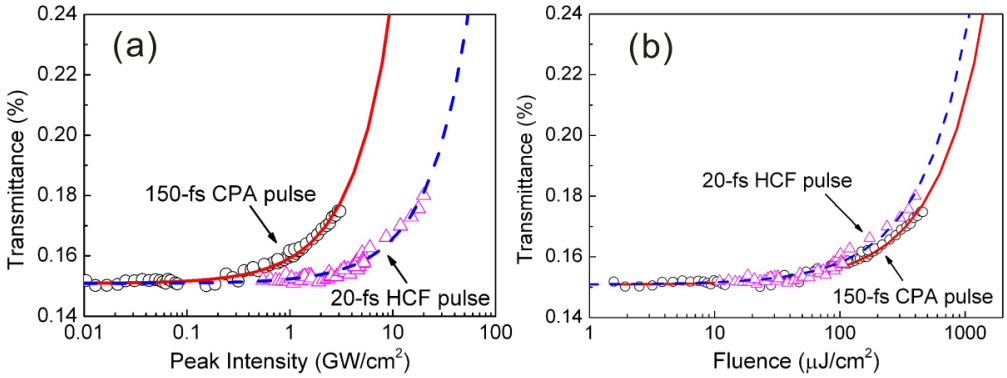

Fig. 3. Experimental (points) and simulated (curves) saturable absorption for the multilayer graphene sample, for both 150-fs (CPA, circles) and 20-fs (HCF, triangles) pulses. Transmittance as function of (a) peak intensity and (b) corresponding fluence. The simulation is based on a sample with 280 layers and an effective scattering time of τ = 4 fs for the carriers at the initial excitation energy.

In order to comprehend the experimental observations, we carried out a series of simulations employing the physical model developed in Ref [14], which had been applied there for the case of excitation by 200-fs near-infrared pulses. In general, the absorption of near-infrared radiation in graphene is dominated by interband excitation, which can be described reasonably well by Fermi's golden rule, where the absorption in graphene is dictated by the electron (hole) occupation probabilities in the conduction (valence) bands. Intraband absorption, found to be important at lower photon energies [30], is not taken into account in the model.

As per Ref [14], we consider only a single carrier energy (corresponding to the center photon energy $\hbar\omega$ of the excitation spectrum). The time-dependent electron (hole) occupation probability function $f_{\hbar\omega/2}$ ($f_{-\hbar\omega/2}$) in each single layer of graphene can be written as:

$$\frac{\partial f_{\hbar\omega/2}(t)}{\partial t} = -f_{\hbar\omega/2}\frac{I(\omega,t)\cdot\pi\alpha/(\hbar\omega)}{D(\hbar\omega/2)\cdot\Delta(\hbar\omega)} + f_{-\hbar\omega/2}\frac{I(\omega,t)\cdot\pi\alpha/(\hbar\omega)}{D(-\hbar\omega/2)\cdot\Delta(\hbar\omega)} - \frac{f_{\hbar\omega/2}}{\tau}, \quad (1)$$

$$\frac{\partial f_{-\hbar\omega/2}(t)}{\partial t} = -f_{-\hbar\omega/2}\frac{I(\omega,t)\cdot\pi\alpha/(\hbar\omega)}{D(-\hbar\omega/2)\cdot\Delta(\hbar\omega)} + f_{\hbar\omega/2}\frac{I(\omega,t)\cdot\pi\alpha/(\hbar\omega)}{D(\hbar\omega/2)\cdot\Delta(\hbar\omega)} + \frac{1-f_{-\hbar\omega/2}}{\tau}, \quad (2)$$

where ω denotes the angular frequency of the incident light, $I(\omega,t)$ the incident light intensity, $\Delta(\hbar\omega)$ the spectral width of the optical pulse, α the fine-structure constant (which determines the "universal" weak absorption in graphene [31]), and τ is an effective scattering time which incorporates both the ultrafast redistribution and relaxation of the carriers due to predominantly carrier-carrier and carrier-phonon scattering, respectively [15, 16, 32]. $D(\pm\hbar\omega/2) = \hbar\omega/(\pi\hbar^2 v_F^2)$ denotes the corresponding combined density of states at the energies $\pm\hbar\omega/2$ (where, for graphene, we take $D(-\hbar\omega/2) = D(+\hbar\omega/2)$), and $v_F = 10^6\ m/s$ is the Fermi velocity. The terms on the right-hand side of the rate Eqs. (1), (2) describe the stimulated emission, absorption and intra-band carrier dynamics, respectively. The numerical solution of Eqs. (1) and (2) yields the time-dependent transmitted pulse intensity (and hence

Optics EXPRESS

also temporal pulse shaping effects), which can then be integrated over time to yield the transmitted pulse fluence. A Gaussian beam profile is assumed for the spatial distribution of the intensity of the pulse, and hence the pulse fluence is obtained by taking the Gaussian-weighted integral over the beam profile. In our case with turbostratic multilayer graphene [25], we assume independent graphene layers and solve Eqs. (1) and (2) for each layer sequentially. To derive the incident pump intensity of each layer, we first calculate the nonlinear absorption in the present graphene layer and use the transmitted intensity as the input for the next layer. We assume the Fermi energy to be zero ($f_{\hbar\omega/2}=0, f_{-\hbar\omega/2}=1$) before the pump pulse arrives, and the sample temperature to be 300 K.The simulated transmittance curves are shown in Fig. 3(a) and 3(b), assuming a Gaussian beam diameter of 2.8 mm and a scattering time of $\tau = 4$ fs. As can be seen, the experimental data are well reproduced for both optical pulse durations, assuming the same value of τ. In order to assess the impact of uncertainties in the precise pump beam diameter, additional simulations were carried out for the beam diameter varying from 2.7 mm to 3.4 mm – in these cases, the values of τ which best reproduced the data ranged from 3 to 5 fs, correspondingly. These deduced scattering times agree well with the lower range of values presented in previous reports and derived by pump-probe and nonlinear-saturable-absorption measurements, which yielded relaxation times ranging from 2 fs to 13 fs [14–16].

The saturation intensity I_s is a commonly cited quantity for saturable absorber applications, defined as the incident intensity that reduces the absorption to half of the unbleached value. Based on the model calculations with $\tau = 4$ fs, we predict saturation intensities for a *monolayer* graphene sample of 28 GW/cm^2 and 148 GW/cm^2 for the CPA and HCF pulses, respectively. Simulations vs. the number of graphene layers show that I_s increases with the number of graphene layers, e.g., the saturation intensities of 100 graphene layers rise to 100 GW/cm^2 and 440 GW/cm^2 for CPA pulse and HCF pulse, respectively. This tendency is as expected, as more incident light power is needed to reach the saturation intensity of deeper layers due to front-layer absorption. Refs [22, 24]. noticed this trend for Bernal-structured several-layer graphene and turbostratic multilayers, respectively. However, two other papers in the literature [12, 17] observed opposite trends, and the authors attributed this behavior to the scattering effect induced by sample defects.

3.2. Discussion of the short- vs. long-pulse regimes

When comparing literature values on saturation intensity (only considering here the case of the photon energy being much higher than the energy of the optical phonons of graphene of 0.2 eV at the Γ point), one notices a significant difference of the values if the pulse duration is higher, respectively lower than the 0.5-ps time scale. For example, for excitation with optical pulses with a photon energy of 0.8 eV, the reported saturation intensity jumps from about 0.5 MW/cm^2 [12, 17, 19] for excitation with pico- and nanosecond pulses to about 250 MW/cm^2 [20, 21] for excitation with 200-fs and 400-fs pulse. The graphene samples' properties (thickness, doping, and defects) contribute, while they cannot account for such huge difference. This situation in the literature is not limited to graphene: For instance, a recent paper on the saturation intensity of black phosphorus has reported a nearly 20 000-times increase from 18 MW/cm^2 to 334 GW/cm^2 if the pulse width decreases from 1.5 ps to 100 fs (here, also the photon energy changed from 0.79 eV to 1.55 eV, respectively, and the sample preparation was different, which accounts, however, only for some of the difference) [33].

Based on the concept that Pauli-blocking-induced absorption changes are responsible for the enhanced transmission at high intensity, one certainly expects a higher saturation intensity for shorter pulses, because a short pulse contains fewer photons than a long one of the same peak intensity and can excite fewer charge carriers (because of that, the pulse energy would be the better quantity to utilize for the comparison of saturation effects, at least as long as

Optics EXPRESS

carrier recombination during the pulse is insignificant). This aspect is, however, still not sufficient to explain the observed differences in the saturation intensity.

Researchers have tried to calculate the saturation intensity I_s and to explain the large differences of the values of I_s in the literature with carrier-relaxation models. Ref [21]. addresses the discrepancies but does not arrive at a reasonable explanation from their model; Ref [12]. includes the carrier longitudinal diffusion into the model and claims that it plays an important role for the long-pulse excitation conditions. In both cases, the models assume a single carrier relaxation rate, and do not investigate different carrier-relaxation pathways. Optical pump-probe experiments have been employed to obtain more detailed information on the carrier dynamics of graphene [32, 34]. The temporal changes of the absorption of the probe pulse reflect different carrier relaxation channels dominant at different pump-probe time delays. Similarly, as to saturable absorption measurements with varied optical pulse width, different carrier relaxation mechanisms must be distinguished for respective saturation intensity interpretations. Basically, two different scenarios apply, depending on the excitation pulse width compared with the demarcation time of roughly 0.5 ps, set by the carrier-phonon scattering time which is on the order of 150 fs to 1 ps as derived by pump-probe studies [35, 36].

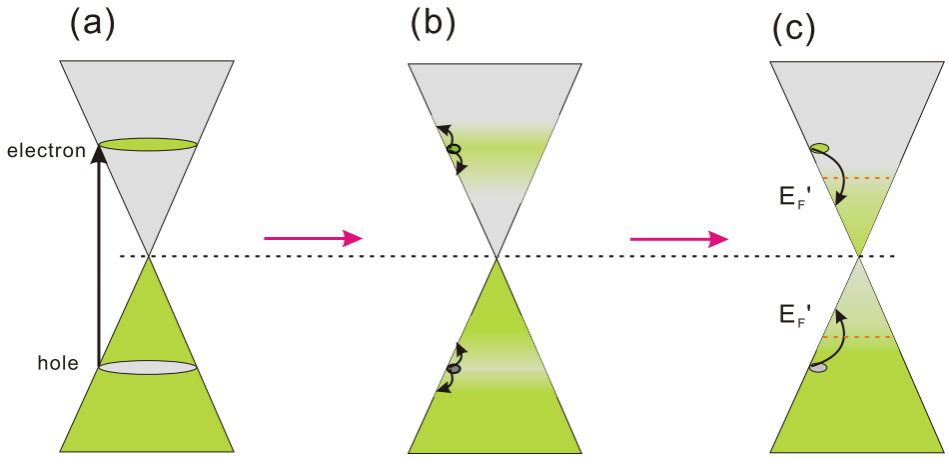

Fig. 4. Schematic depiction of the optical excitation (a) and carrier relaxation (b, c) in graphene, with (b) carrier redistribution due to carrier-carrier scattering during a short time scale after the excitation, and (c) carrier relaxation due to carrier-phonon scattering with carrier accumulation in the bottom (top) of the conduction (valance) band on a longer time scale. Note that, for our situation, we find step (b) to occur effectively already during excitation.

If the optical pulse is much longer than the demarcation time scale (so called long-pulse excitation), one expects the charge carrier distribution to develop into quasi-equilibrium within the optical pulse duration. The photo-excited carriers (Fig. 4(a)) first redistribute among each other through elastic carrier-carrier scattering (Fig. 4(b)), then exchange energy with the lattice via carrier-phonon scattering (Fig. 4(c)) [15, 34, 36], eventually accumulating at the bottom of the conduction respectively the top of the valance band as a warm carrier ensemble. The accumulated carriers are characterized by two quasi-Fermi-Dirac distributions, where the Fermi levels are determined by the balance between optical excitation and electron-hole recombination. The carrier temperature (which will be higher than the lattice temperature) mainly depends on the energy deposited by the optical excitation and on the pulse duration: the longer the pulses, the lower the carrier temperature tends to be. As a consequence of this moderate carrier temperature, Pauli blocking of the optically coupled band states becomes active only for sufficiently high optical power when the quasi-Fermi levels are lifted to the range of half the photon energy $\pm \hbar\omega/2$. This scenario applies to the

Optics EXPRESS

model developed in Ref [17]. when pico- and nanosecond pulses, or even CW light, are used in the saturable absorption measurements [12, 17, 19, 25]. Basically, the conduction band states which need to be filled, are those below and up to the optically coupled states (the mirror image applies to the holes). That this does come at an only moderate cost in pulse energy is a consequence of the fact that the density of states rises rather slowly with energy (with a linear energy dependence, starting at zero). The band filling by the optical excitation competes with electron-hole recombination, though, which is believed to proceed, dependent on the carrier density according to a bimolecular recombination scenario, on a time scale of 1-15 ps for the carrier densities relevant here [32, 37].

In contrast, if the optical pulse is much shorter than the demarcation time scale, carrier cooling remains ineffective during the pulse and the total deposited photon energy remains in the carrier ensemble. Because of the high efficiency of carrier-carrier scattering, the evolution of the quasi-Fermi-Dirac distributions will proceed fast (although the process will probably not be complete during the 20-fs time scale [16, 35, 37], see next section). The effective carrier temperature will be very high, and electrons populate band states not only below and at the optically coupled states, but also above them (inversely for holes) where the density of states is high [16, 34, 35]. A much higher carrier density than in the long-pulse regime is needed to reach substantial absorption saturation. This situation applies to the model developed in Refs [14, 21].

Comparing our CPA and HCF pulse measurements, one might have expected intuitively that the pulse fluence required to obtain saturation would be lower for the HCF pulse, as the corresponding peak intensity is much higher and the carriers have less time to redistribute away from the excitation energy. That this is not what is observed (both experimentally and in the simulations) is due to two reasons: (i) the scattering time of ~4 fs determined here is still much shorter than the 20-fs HCF pulse, so that the redistribution effects are still fast on the time scale of the pulse; (ii) the broader optical bandwidth of the HCF pulse populates a broader initial carrier energy distribution. Nevertheless, as the optical bandwidth is increased, one should expect that the relative effect of redistribution will be reduced at least at the low-energy side of the pulse spectrum, although for the case of graphene (where the available electron energy states begin at zero energy) this will only become significant if the pulse bandwidth becomes comparable to the carrier frequency, i.e., for a pulse duration below 10 fs.

3.3. Intensity-dependent transmittance spectra

In order to gain further insight into the carrier dynamics associated with saturable absorption, here we present spectrally resolved measurements using the HCF pulses. As detailed above, this was achieved using a dual-channel spectrometer in place of the photodetectors (again with a sample beam, and reference beam for normalization, see Fig. 2. Figure 5(a) presents normalized differential transmittance spectra for a set of intensities, i.e., where the differential intensity is normalized relative to the low-intensity (3 GW/cm^2) transmittance spectrum (a reference intensity spectrum of the HCF pulses over the full wavelength range is shown in Fig. 5(c)). As can be seen, as the saturable absorption sets in, it is much more pronounced on the low-energy side of the spectrum, reaching a level of 20-25%, while a weaker effect for the higher energy side only becomes significant relative to the noise floor at higher incident power. Hence, the transmittance change of ~13% presented above (Fig. 3) is not evenly distributed over the pulse spectrum. Note that care was taken to achieve near-transform-limited pulses at the sample, to minimize any possible spectro-temporal effects due to chirp. Considering the non-uniform intensity spectrum of the input pulses (Fig. 5(c)), the pulse spectral intensity has a maximum at the high-energy side, and hence the wavelength dependence of the transmittance spectra cannot be justified by the directly excited carrier energy distribution. This result also supports that there is significant carrier energy redistribution during the duration of the 20-fs optical pulse, consistent with the effective scattering time of τ = 4 fs deduced by modeling of the data in Sec. 3.1.

Optics EXPRESS

In order to investigate numerically whether the pronounced spectral dependence observed in Fig. 5(a) can be reproduced by the assumption of a fully thermalized carrier plasma (and hence by assuming near-instantaneous elastic carrier redistribution), we employ a simplified theoretical approach to calculate the transmittance spectra. We first calculate the optical excitation densities and absorption in each layer of the multilayer graphene using the model developed in Sec. 3.1, then derive the total carrier energy (equal to the absorbed pulse energy) and carrier density (absorbed fluence divided by photon energy), both for each layer. Unlike the approach of Sec. 3.1, where the lateral spatial profile of the optical beam has been taken into account explicitly, we neglect it here and assume a simple disk-shaped profile, taking half of the on-axis power density to represent the averaged power density. As stated before, previous pump-probe studies of graphene showed that the time scale for inelastic carrier-phonon scattering is ≥100 fs [35], and hence we assume that only elastic carrier-carrier scattering and energy redistribution occur on the time scale of the HCF pulse. For each layer, we calculate the quasi-Fermi-Dirac distributions $f(E)$ for the conduction/valence bands for the respective carrier densities and deposited energies [14], i.e., we determine the chemical potential $\mu_{e,h}$ and temperature $T_{e,h}$ conserving both total electron/hole number and energy per layer. This implies that thermalization of the carrier ensemble is complete but that no energy exchange has occurred with the lattice. The absorption of each graphene layer is then determined by the universal absorption of graphene modulated by the electron/hole occupation probabilities. The spectrum of the total transmittance through all graphene layers is calculated as:

$$T(\hbar\omega) = \prod_n \left\{1 - \pi\alpha \cdot \left[f_n^{ve}(-\hbar\omega/2) - f_n^{ce}(\hbar\omega/2) \right] \right\} \tag{3}$$

where $\pi\alpha$ defines the universal absorption of graphene sheet, $f_n^{ve}(-\hbar\omega/2)$ represents the electron quasi-Fermi-Dirac distribution at energy $-\hbar\omega/2$ in the valance band of the n^{th} graphene layer, and $f_n^{ce}(\hbar\omega/2)$ the is corresponding electron quasi-Fermi-Dirac distribution at energy $\hbar\omega/2$ in the conduction band. Equation (3) takes both absorption and stimulated emission into account [14].

In Fig. 5(b), we present the calculated occupation probability of the conduction/valence band in layer 1, 50, 100 and 200 for an incident intensity of 15 GW/cm^2. One notices that the occupation probability (and hence the degree of saturation) gradually decreases up to ~100 layers and deeper layers don't exhibit saturation anymore. The dash-doted lines in Fig. 5(a) are the calculated normalized differential transmittance spectra $\Delta T/T$ for intensities of 18, 15, 9 and 4 GW/cm^2 (normalized to the 3-GW/cm^2 spectrum for direct comparison with the measurements). While the overall degrees of saturation observed in the experiment are well reproduced by the calculation (without fitting parameters), the spectral dependence is clearly more pronounced in the experiment than in the simulation. This leads us to conclude that the transmittance spectra are not determined/dominated by fully thermalized carrier distributions. Apparently, the deviations of the calculated from the experimental spectra are the result of a relaxation process which, although extremely fast (τ = 4 fs, see Sec. 3.1), still leaves its traces in the spectral response of the absorption saturation.

Interestingly, qualitatively similar spectral dependencies as in our experiment were observed in pump/probe measurements on photo-excited thin-layer graphite and on single-layer graphene [16, 37]. For several tens of femtoseconds after excitation, signatures of the initial excitation spectrum by the pump pulses survived in the measured probe spectra and produced features which were more pronounced during non-equilibrium than in the equilibrated cases. Against this backdrop, it is not surprising that our data show characteristics which indicate deviations from thermal distributions. It is rather more surprising that the analysis of our data in Sec. 3.1 yields such a short relaxation time constant of 4 fs, if the

Optics EXPRESS

development of the spectra in Refs [16, 35]. extends into the tens of fs. Probably, the relaxation is multi-scaled in time, with an initial high rate of energy redistribution followed by slower processes thereafter. Carrier multiplication and Auger processes are likely to play an important role in the dynamics [35].

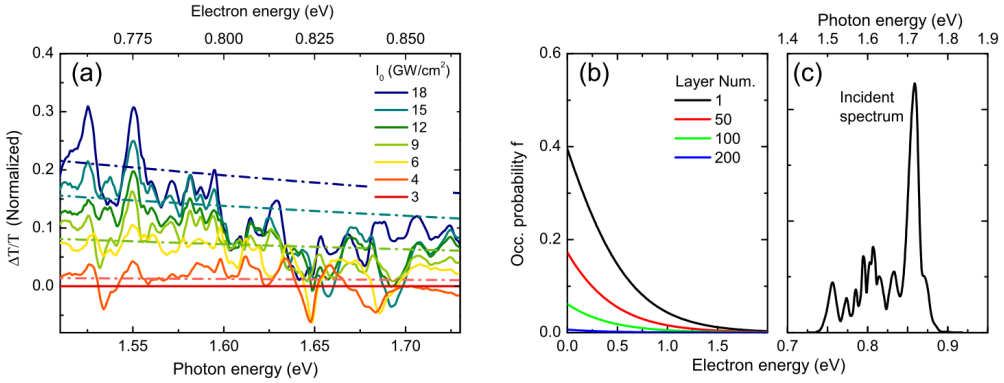

Fig. 5. (a) Normalized differential transmittance spectra for the 20-fs HCF pulses for different incident intensities, as indicated in the legend; the dash-dotted lines are the calculated normalized differential transmittance spectra for excitation intensities of 18, 15, 9 and 4 GW/cm^2. (b) Calculated Fermi-Dirac distributions following elastic carrier redistribution in the 1st, 50th, 100th and 200th graphene layer, for an excitation intensity of 15 GW/cm^2. (c) Magnified spectral region about the incident HCF intensity spectrum.

3.4. Potential simulated performance and pulse reshaping effects

In this last section, we employ the theoretical model and the graphene parameters determined from the analysis above to explore the potential of multilayer graphene as saturable absorber with a more suitable number of layers. While the peak normalized transmittance change due to saturable absorption presented in Sec. 3.1 (Fig. 2) was only ~13%, those measurements were limited to a peak intensity <30 GW/cm^2, and the use of a ~280-layer sample leads to only a weak saturation of the deepest layers. Here we consider a sample composed of 100 layers, which should have a linear (low-intensity) transmission of 10%. Moreover, as the damage threshold of graphene has been determined to be as high as 300 GW/cm^2 [14, 18, 29], we simulate intensities up to 100 GW/cm^2. The simulations are carried out according to the model presented in Sec. 3.1 for a 20-fs optical pulse duration and effective scattering time of τ = 4 fs. As the integration of the equations yields the time-dependent transmission, we can also inspect here the expected temporal reshaping effects.

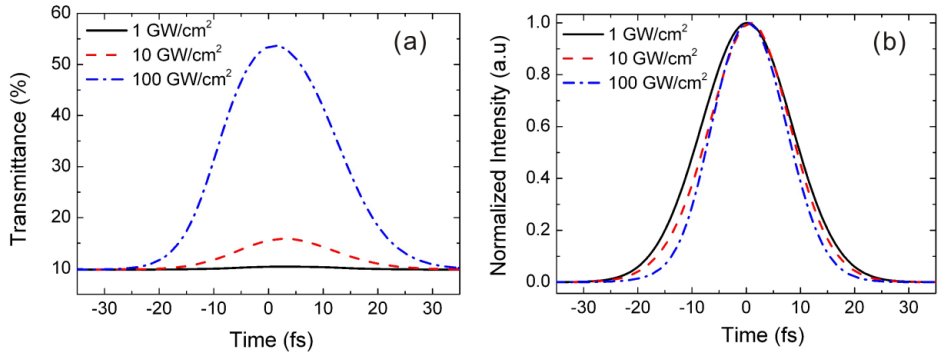

Fig. 6. Time-dependent saturable absorption and pulse shaping effects predicted by simulations for a 100-layer graphene structure and 20-fs optical pulse duration (τ = 4 fs). (a) Temporal transmittance, and (b) corresponding normalized intensity profiles.

Optics EXPRESS

The results are depicted in Fig. 6, both in terms of the (a) time-dependent pulse transmission and (b) normalized temporal intensity. For the low-intensity simulation (I_0 = 1 GW/cm^2), the effects of saturable absorption and pulse re-shaping are barely perceptible, as expected. In going to the highest intensity (I_0 = 100 GW/cm^2), however, the predicted peak transmittance reaches above 50%, compared to 10% at the temporal wings, i.e. corresponding to an improvement in optical contrast of ~5. This case corresponds to a total pulse energy transmittance of 42%, which could well be of practical value for certain experiments (note that from the discussion of the TPA in SiC, one would need a different substrate to avoid the TPA effect). In Fig. 6(b), one can see that the temporal transmittance change also results in noticeable pulse shortening, from a duration of 20 fs down to 16 fs. Although the effective scattering time of 4 fs results in an almost instantaneous saturable absorption response, one can still observe a small asymmetry between the lead and trailing edges of the pulse, due to the residual carrier accumulation in the latter case. While the degree of pulse shortening here is lower than for the situation with a plasma mirror (where the trailing edge is essentially truncated by the plasma losses [11]), it should still provide the additional benefit of improved time resolution/steep excitation edge for experiments.

4. Conclusion

We have experimentally characterized the saturable absorption of ~280-layer turbostratic graphene (on SiC substrate) using near-infrared optical pulses with 150-fs and 20-fs duration. The experimental observations have been well reproduced by the theoretical model with an effective scattering time of 3-5 fs which we associate with (elastic) carrier-carrier scattering that redistributes the excited carriers over a broad energy range (and hence strongly depopulates the directly excited energy region). A comparison of the data shows that the shorter pulse still has essentially the same saturation fluence, despite the higher peak intensity. This can readily be understood, as the increase in the instantaneous rate of state filling is accompanied by the excitation of a broader band of carrier energies, coupled with the fact that the effective carrier scattering time is still significantly shorter than 20 fs. Experiments with even shorter pulses (i.e. <10 fs), however, should show a lower saturation fluence, both by approaching the time scale of the redistribution as well as the spectral width of the redistributed carriers. The spectrally resolved measurements showed a strong wavelength dependence (with a significantly larger saturation on the low photon-energy side), which we could not reconcile by assuming a simple Fermi-Dirac distribution after initial elastic carrier-carrier scattering. Simulations for a 100-layer sample indicate that an experimentally useful improvement in the optical contrast of pulses (e.g. with a duration of 20 fs and peak intensity of 100 GW/cm^2) should be achievable, as well as some temporal compression. It is interesting to compare graphene with conventional semiconductors as a saturable absorber in this pulse regime. While graphene offers ultra-broadband applicability at NIR/VIS photon energies and provides absorption for the full frequency bandwidth even of extremely short femtosecond pulses, and although it has a very strong absorption per monolayer, we see that the ultrafast redistribution over a large energy range of available states leads to a rather high saturation intensity for near-infrared pulses, even with a duration as short as ~20 fs. The saturation intensity can be significantly reduced in conventional semiconductors (or their nanostructures), by excitation near the band edge, such that redistribution does not reduce the charge accumulation and Pauli blocking in the excitation bandwidth as strongly. This raises the question of whether doping of the graphene layers could be advantageous for near-infrared pulses, to generate a pre-existing Fermi level (in either the valence or conduction band) in order to ameliorate this issue compared to undoped graphene. Similarly, an interaction between the graphene layers might be useful, because it would introduce a bandgap which would facilitate the achievement of Pauli blocking of the optically coupled band states.

Optics EXPRESS

Acknowledgments

The Italian contribution to the work was supported in part by the European Union's Seventh Framework Programme under grant agreement n° 604391 of the Graphene Flagship. The German team benefitted from funding by the Hessian excellence initiative LOEWE, project *Sensors Towards Terahertz*. H.G.R. thanks Xuan (Betty) Sun and Prof. Dr. Xi.-Cheng Zhang, University of Rochester, for experimental help during a sabbatical at the early stage of this research project.